Philosophical Magazine

ISSN: 1478-6435 (Print) 1478-6443 (Online) Journal homepage: http://www.tandfonline.com/loi/tphm20

Effects of porosity on the measured fracture energy of brittle materials

L. J. Vandeperre , J. Wang & W. J. Clegg

To cite this article: L. J. Vandeperre , J. Wang & W. J. Clegg (2004) Effects of porosity on the measured fracture energy of brittle materials, Philosophical Magazine, 84:34, 3689-3704, DOI: 10.1080/14786430412331293522

To link to this article: https://doi.org/10.1080/14786430412331293522

Published online: 22 Aug 2006.

Philosophical Magazine, 1 December 2004
Vol. 84, No. 34, 3689–3704

Taylor & Francis
Taylor & Francis Group

Effects of porosity on the measured fracture energy of brittle materials

L. J. Vandeperre, J. Wang and W. J. Clegg†

Ceramics Laboratory, Department of Materials Science and Metallurgy, University of Cambridge, Pembroke Street, Cambridge CB2 3QZ, UK

[*Received 8 September 2003 and accepted in revised form 15 July 2004*]

Abstract

Although it is known that growing cracks will interact with pores, it is unclear whether the magnitude of this effect is sufficient to influence the fracture energy. To study this, experiments have been carried out where cracks have been grown through simple distributions of pores in poly(methyl methacrylate). These show that the applied force required to grow the crack between two pores can be greater than that required to grow the crack in the pore-free material. Direct observation during crack growth shows that this increase in applied force is associated with the crack front becoming curved. Based on these observations, the effect of equiaxed pores on the fracture energy of brittle materials has been quantitatively described. The analysis predicts how the relative fracture energy should be influenced by the pore volume fraction, and that it should be independent of the size of the pores or the fracture energy of the matrix. These predictions give good agreement with experimental measurements in different ceramic materials, in which the microstructure of the matrix surrounding the pores does not change with pore volume fraction.

§ 1. Introduction

Although the effects of porosity on variables such as elastic modulus and thermal conductivity can be accurately, and quite simply, described, this is not so for the fracture energy with different trends in behaviour being observed in different systems (Rice 1998). It is therefore not surprising that there are several different analyses to explain these observations.

It has been suggested that the fracture energy should vary as the elastic modulus, as the fracture energy is equal to the elastic energy stored in a body at failure (Wagh *et al*. 1993, Arato 1996). However, the condition for cracking is given by the energy changes that occur upon incremental crack advancement (Griffith 1920, Lawn and Wilshaw 1975) rather than upon cracking across the whole sample. The condition under which this might be true can be seen by considering the failure stresses and strains in a porous and dense body. These can be written as (Lawn and Wilshaw 1975)

$$E_{\mathrm{d}}\varepsilon_{\mathrm{d}} = \sigma_{\mathrm{d}} = \left[\frac{E_{\mathrm{d}}R_{\mathrm{d}}}{Yc_{\mathrm{d}}}\right]^{1/2} \tag{1}$$

†Author for correspondence. Email: wjc1000@cam.ac.uk.

Philosophical Magazine ISSN 1478–6435 print/ISSN 1478–6443 online
http://www.tandf.co.uk/journals
DOI: 10.1080/14786430412331293522

and

$$E_p\varepsilon_p = \sigma_p = \left[\frac{E_p R_p}{Y c_p}\right]^{1/2}, \tag{2}$$

where E is Young modulus, R is the fracture energy, ε is the strain at failure, σ is the nominally applied stress at failure, c is the size of the critical defect, Y is the shape factor for that defect, and the subscripts indicate whether these are for the dense, d, or porous, p, body. Dividing equation (1) by equation (2), the relative fracture energy is found as

$$\frac{R_p}{R_d} = \left(\frac{E_p}{E_d}\right) \cdot \left(\frac{c_p}{c_d}\right) \cdot \left(\frac{\varepsilon_p}{\varepsilon_d}\right)^2. \tag{3}$$

Since the critical defect size in a given sample does not affect the fracture energy, the relative fracture energy can be equal to the ratio of the Young moduli only if the strains to failure for the porous body and the dense body are the same. No attempt has been made to justify this assumption, and experiments do not support it (Datta *et al.* 1988, Shigegaki *et al.* 1997).

Using a description of cleavage fracture (Gilman 1959), Rice has suggested that the fracture energy should change with porosity in the same way as the elastic modulus because the surface energy and hence the fracture energy of a material is determined by the strength of its bonds, which is related to the elastic modulus (Rice 1998). However, this assumes that the measured fracture energy of a material is due simply to that required to create two new surfaces. This is approximately true in only very few materials such as diamond. Even in ceramics, microstructural effects such as grain bridging can increase the fracture energy by orders of magnitude above the surface energy. Moreover, it is unclear how the presence of porosity, which does affect the measured macroscopic elastic modulus, would alter the bond strength or surface energy of the matrix material.

Alternative descriptions of the effect of porosity on the fracture resistance of brittle materials consider the change in the area fraction of material in the crack plane that must be broken. For a uniform distribution of pores in a brittle matrix, the area fraction of material in a random plane is equal to the relative density, and one might therefore expect the fracture energy to be directly proportional to the relative density. However, in reality, the relationship between the overall pore volume fraction and the area fraction of pores in the crack plane is often more complex than this. One approach is to assume that the crack will grow on the plane with the minimum area fraction of solid material. This predicts that the relative fracture energy should vary with porosity according to (Rice 1998)

$$\frac{R_p}{R_d} = k(1 - P)^n, \tag{4}$$

where R_p is the fracture energy of the porous material, R_d is the fracture energy of the matrix and n and k are constants, which take into account the details of the shape and distribution of the pores and are often considered as variables to be fitted to the experimental data.

Porous materials are often made by partially sintering a powder compact. Here, failure occurs by the fracture of the necks that develop during sintering. The situation is more complex than before but there are two limits. The first is where the body

contains no pores so that the fracture energy is equal to that of the dense material. The other limit is in the unsintered compact, for which the fracture energy is negligible, although not zero (Johnson *et al.* 1971). Following the idea that the fracture energy should scale with the amount of material in the crack plane, the fracture energy is predicted to vary according to (Lam *et al.* 1994):

$$\frac{R_p}{R_d} = \left(1 - \frac{P}{P_g}\right)^{n'}, \tag{5}$$

where P_g is the density of the green body and n' is a constant. Lam *et al.* found that, for their data, n' was equal to 1, that is the fracture energy varied linearly between the two limits. And because the minimum solid area approach gives a good description of the elastic modulus, the result is again that one expects the fracture energy to vary with porosity in the same way as the modulus.

Some results support this view, although when more data are considered simultaneously, the results are less convincing (Rice 1998). To illustrate this, figure 1 shows published data for the fracture energy of aluminium oxide with a pore volume fraction less than 0.2. The fracture energy varies between 10 and 50 J m^{-2} and the scatter suggests that there is no evidence for a correlation with porosity. As pointed out by Simpson (1973) changes in other microstructural variables can obscure changes due to porosity. For example, the large scatter apparent in figure 1, where the fracture energy is plotted against porosity, is not present when the fracture energy is plotted against grain size, suggesting that the fracture energy of nearly dense partially sintered aluminium oxide is influenced more strongly by the grain size than by the volume fraction of pores (Wang *et al.* 2001). It is thus essential to

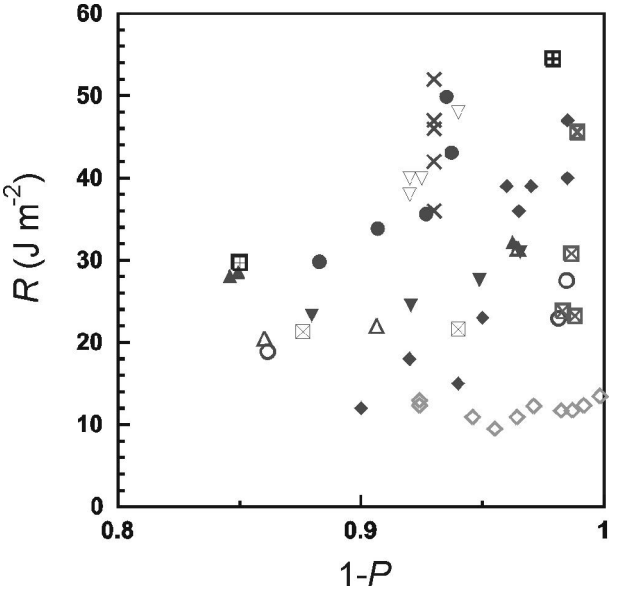

Figure 1. Literature data for the fracture energy of various partially sintered aluminas: (▲) Lam *et al.* 1994; (▽) Daghleish *et al.* 1976; (◇) Coppola and Bradt 1973; (×) Perry and Davidge 1973; (◇) Simpson 1973; (○ △ ▽ ●) Ostrowski *et al.* 1998, Ostrowski and Rödel 1999; (⊠ ⊞) Wang *et al.* 2001.

eliminate any effects due to the microstructure of the matrix changing at the same time as the pore volume fraction. To do this, Boccaccini (1999) studied glasses where the porosity was controlled by mixing in hollow glass spheres before densification. Unfortunately, only the strength of the glasses was measured, so that the fracture energy cannot be determined without assuming the size of the critical flaws in the sample. It is therefore unclear at present how the fracture energy varies with porosity when the microstructure of the material between the pores remains unchanged.

Analyses where the fracture energy is proportional to the average area of material in the crack plane assume the interaction between cracks and pores is negligible. The pores simply reduce the amount of material that must be broken. However, it is known that pores interact with growing cracks. Bethge (1962) found evidence of cracks circumventing pores in crystals of sodium chloride. Similar effects have been observed in glasses (Kerkhof and Sommer 1964, Peter 1968). It has also been suggested that the fracture tails observed on the fracture surface as the crack grows away from the pore are due to the crack growing around the pore, rather than simply growing through it (Passmore *et al.* 1965). The tail being produced as the segments of the crack that have grown around opposite sides of the pore do not meet again on quite the same plane.

Lange (1970) has interpreted these observations by attributing a line energy to a crack front. Assuming that the stress required to grow the crack between any obstacles was equal to that needed to bow the crack front into a semi-circular shape, he estimated the strength of a brittle material containing obstacles, which might be either pores or hard particles. He predicted that, for a given volume fraction of obstacles, a fine dispersion of particles would give a stronger body than one containing a coarser dispersion. However, this was not consistent with experiments on glasses containing alumina particles (Lange 1971).

To overcome this problem he suggested that the line energy of the crack front might vary with its shape. In later work by Evans and by Green, it was suggested that finer particles could be less effective at preventing the movement of the crack front if the crack were able to penetrate the smaller particles so that the crack could escape before the crack front had become semi-circular in shape (Evans 1972, Green 1983). No criterion was given to determine when particle penetration would occur. Furthermore, there is evidence from dynamic tests that fine pores interact with propagating cracks in the same way as coarse pores and these observations also indicate that pores do not pin cracks, but appear to exert a drag force on them (Green *et al.* 1977). Despite this, there are no experiments to show whether the magnitude of this interaction is significant.

The aim of this paper is therefore twofold. Firstly, to establish how the fracture energy of a brittle material varies with the volume fraction of pores. Secondly, how cracks interact with pores and, in particular, to quantify whether the magnitude of this interaction is sufficient to influence the fracture energy.

§ 2. Experiments

2.1. *Variation of the fracture energy of alumina with porosity*

Alumina samples were made by slip casting slurries of an alumina powder (Sumitomo, AKP30) dispersed in water with the aid of a dispersant (Dispex A40, Ciba Speciality Chemicals). Volume fractions of pores in the final sintered sample ranging from 0 to 0.6 were obtained by adding starch particles to the slurry, which

were then slip cast and heated to 1550°C for 1 h. Starches with mean particles sizes of 5 μm (rice starch), 15 μm (corn starch) and 45 μm (potato starch) were used. The starch particles burn away during heating in air leaving pores, which remain after sintering. All samples underwent the same sintering schedule, and had the same average grain size (3 μm).

The fracture energies were determined by calculation from the fracture toughness as measured using a single edge notch beam (SENB) test. However, to confirm these results, fracture energies were also measured directly with a sample devised by Tattersall and Tappin (1966).

2.2. *Model experiments for the interaction of cracks with pores*

To enable direct observation of the interaction of a crack with pores, model experiments were conducted on a brittle transparent polymer, poly(methyl methacrylate), PMMA. In a first set of experiments, pores were introduced into the sides of grooved double cantilever beam (DCB) specimens by carefully drilling a hemispherical hole or a cylindrical hole with a hemispherical end cap into each side of the sample (see figure 2(*a*)). Subsequently, a crack was grown towards the two pores by applying a moment to the cantilevers and the interaction of crack and pores was observed while measuring the moment, M, required to propagate the crack. To enable comparison between samples of slightly varying dimensions, the moment was expressed as an apparent crack driving force, G_{app}, using the standard expression for the constant moment test (Sorensen *et al.* 1998)

$$G_{\text{app}} = \frac{12M^2}{EBbH^3}, \tag{6}$$

where E is Young modulus, B is the sample thickness, b is the remaining thickness in the grooved region, and H is the width of the beams.

To study the effect of the pore distribution, holes were drilled into specimens perpendicular to the plane of expected crack growth, and a crack was grown through the pores by wedging (figure 2(*b*)).

§ 3. Results and discussion

3.1. *Fracture energy variation with porosity in aluminium oxide*

Figure 3 shows the variation of the fracture energy of alumina with porosity as measured with a single edge notch bend test and as measured with samples containing a chevron notch. While there is a tendency for the results of the single

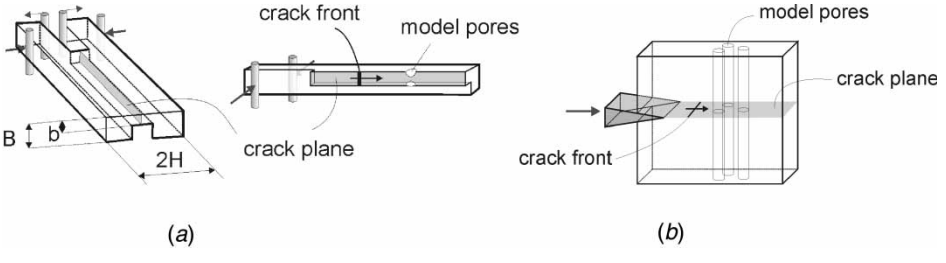

Figure 2. Test configurations for the model experiments: (*a*) double cantilever beam test (Sorensen *et al.* 1998), (*b*) wedging.

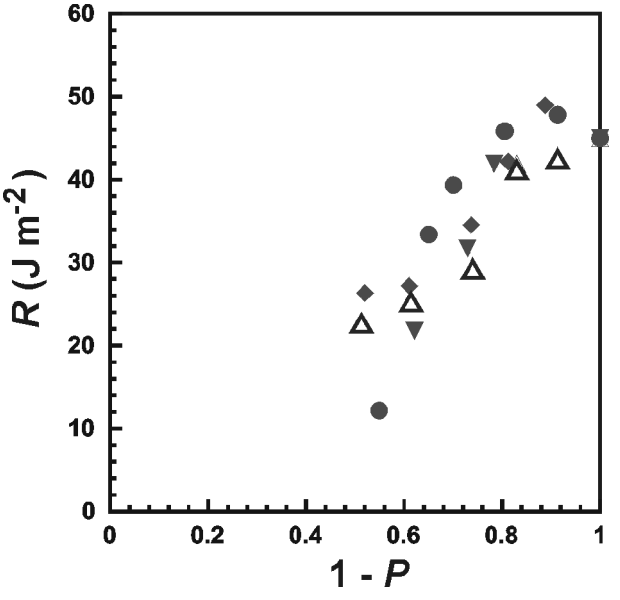

Figure 3. Experimental results for the fracture energy of alumina versus relative density, $1-P$, measured either using the SENB technique (corn starch ●, rice starch ♦, potato starch ▼) or by directly measuring the energy required to break the sample (corn starch △). The average grain size of the materials made with fugitive inclusions was 3 μm.

edge notch bend to be slightly higher, the trends in the variation of fracture energy are entirely similar and most measurements were therefore made with the simpler SENB technique.

In these materials, where the microstructure of the matrix is the same, the fracture energy remains approximately constant at 45–50 J m^{-2} until the pore volume fraction exceeds about 0.15–0.25. In fact, the fracture energy appears to be slightly higher in samples with a low volume fraction of porosity than for dense samples. The absolute value of the fracture energy measured here also agrees well with the values observed in the literature for alumina with a similar grain size. Further, partially sintered alumina of similar density made previously (Wang *et al*. 2001) was measured to have a fracture energy of approximately 20 J m^{-2}. Consistent with the difference in measured fracture resistance, these two types of porous materials also behave very differently when subjected to thermal shock, cracks growing much deeper into the partially sintered bodies (Yuan 1999).

Hence, once the effect of the changes in grain size is removed from data of fracture energy versus porosity, the fracture energy of alumina appears to remain approximately constant as the volume fraction of pores is increased up to a volume fraction of 0.15–0.25, after which the fracture energy falls rapidly with porosity.

Figure 3 shows that the fracture energy is not strongly influenced by the size of the pores, at least in the range studied, similar values being obtained for materials with small pores (about 5 μm, rice starch) as for materials with larger pores (about 45 μm, potato starch).

Similar observations have been made in silicon nitride (Yang *et al*. 2002), silicon carbide (Lankmans 1997) and gadolinium oxide (Case and Smyth 1981). As shown

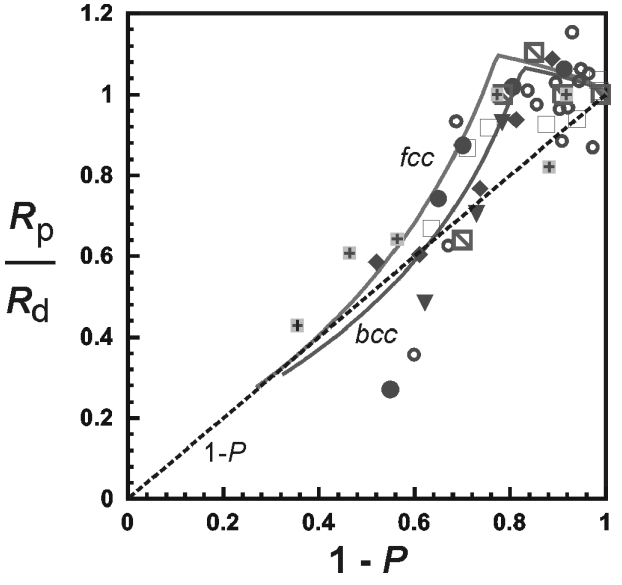

Figure 4. Fracture energy normalized by the fracture energy of dense material: Al_2O_3 (corn starch ●, rice starch ♦, potato starch ▼, and partially sintered □), SiC (▪, Lankmans 1997), Si_3N_4 (▧, Yang *et al.* 2002), Gd_2O_3 (○, Case and Smyth 1981), together with predictions given in the text.

in figure 4, when plotted as the ratio of the fracture energy of the porous material over the fracture energy of the most dense material with the same grain size, it is found that the general trend with porosity is quite similar for a wide range of materials, irrespective of the magnitude of the fracture energy of the matrix, that is it is a relative effect. Unfortunately, not all the data available in the literature for the variation of the fracture energy with porosity could be included in this plot as grain sizes were not always reported.

3.2. *Observations of crack growth in the model system*

Figure 5(*a*) shows how the moment normalized for the sample dimensions, or the apparent crack driving force, varied in a PMMA sample with just two hemispherical pores. Before the crack reaches the pores, a constant value of the crack driving force is observed, which is equal to the fracture energy of the dense matrix. Upon reaching the pores, the crack is observed to accelerate, causing the measured moment to decrease. Once the crack reaches the line connecting the centres of the pores, the measured moment starts to increase and, as is clear from the fracture surface shown in figure 5(*c*), the crack front becomes curved as it spreads around the two pores.

Eventually, the crack reaches a point where it has spread around the boundary of both pores and breaks away. From figure 5 it can be seen that the moment needed to drive the crack into this position is slightly higher than that needed to propagate the crack in the dense matrix. There is then a burst of crack growth as the crack breaks free of the pores, and the moment decreases to the value required for cracking in the dense material before the crack had reached the pores.

If the pores are elongated (see figure 5(*b*)), the process is similar and again the crack only breaks away from the pores when it has spread around the entire pore boundary. However, the maximum length of the crack front at this breakaway point

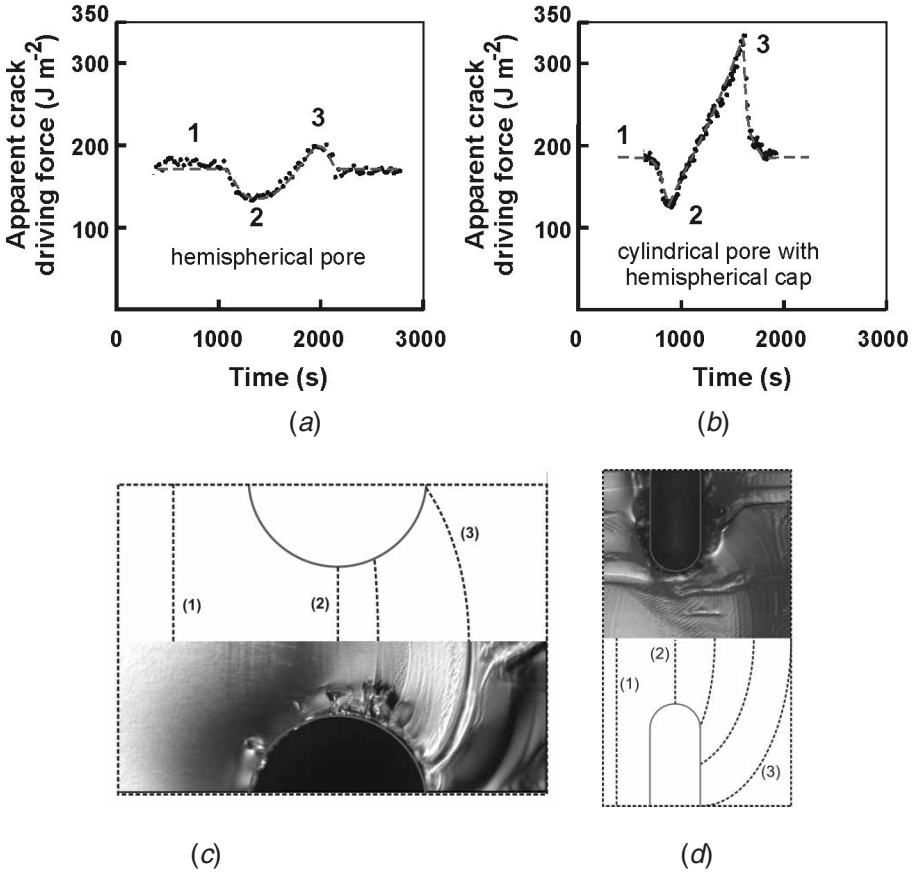

Figure 5. (*a*) Moment normalized for sample dimensions (or apparent crack driving force) as a function of time while a crack is driven through two hemispherical pores. (*b*) Moment normalized for sample dimensions as a function of time while a crack is driven through two elongated pores with hemispherical end caps. (*c*) Fracture surface of a sample with hemispherical pores in its sides compared with calculated crack front positions. (*d*) Fracture surface of a sample with elongated pores in its sides compared with calculated crack front positions. In both images the pore diameter is 1 mm.

is much greater than for the hemispherical pores and the increase in driving force is consequently much greater.

In previous attempts to account for the effect of the interaction of pores and cracks, the curving of the crack front was attributed to the crack front being pinned, that is not being able to move along the pore boundary, and that break-away would occur when the pinned crack grew into a semi-circular shape (Lange 1970). However, it appears from the fracture surfaces that the crack front is never truly pinned. Rather, while the crack front moves forward midway in between the pores, it follows the pore boundary near the edges by approximately the same amount. The curving of the crack front therefore appears to occur because the direction of crack propagation is different on the pore boundary than in the centre between the two pores, which causes the edges of the crack front to lag behind the centre. To confirm this,

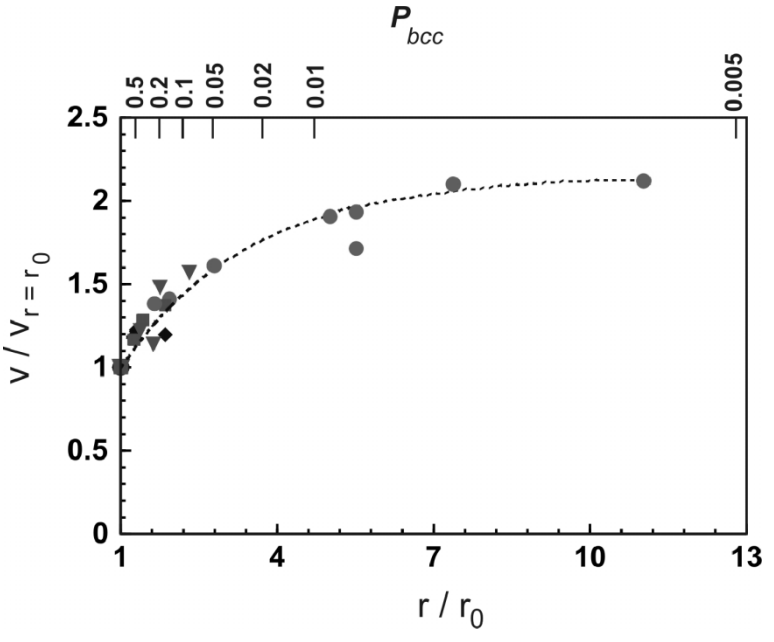

Figure 6. Relative progress of the crack front, v, divided by the progress of the crack front on the pore boundary, $v_{r=r_0}$, as a function of the distance from the centre of the pore, r, normalized by the pore radius, r_0, or as a function of the pore volume fraction, P, for a bcc pore distribution. Data shown as (•) were measured on a fracture surface of a dynamic test shown in Kerkhof and Sommer (1964), while all other data were measured on fracture surfaces of quasi-static tests as shown in, for example, figure 5 or figure 7.

measurements were made of the relative change in position of the crack front in the centre between two pores and on the pore boundary. The results are shown in figure 6, and they confirm that the difference in distance travelled on the pore boundary relative to the distance it has travelled in the centre is often small (except for extremely low pore volume fractions). That is, the observed curvature is indeed mainly due to the difference in the direction of crack propagation on the pore boundary compared with the direction of crack propagation between the pores while each segment of the crack front propagates at a constant rate. Comparison of the data collected from our quasi-stationary tests agrees well with data collected on an image obtained after a fast fracture test, indicating that the speed of crack propagation does not alter the mechanism of interaction.

In the experiments described above, the crack could only escape from the single set of pores once it had spread entirely around the pore boundary. However, as the volume fraction of pores is increased, a crack front spreading around two pores impinges on a pore ahead of it before reaching this position. As illustrated in figure 7, this reduces the maximum length of the crack front because while the curvature of the crack front is developing it cuts into pores ahead of its tip and is divided into smaller segments.

Having established how cracks interact with pores and which features on the fracture surface are evidence for this interaction, the fracture surfaces of the alumina were examined to confirm that cracks interact with pores in a polycrystalline ceramic

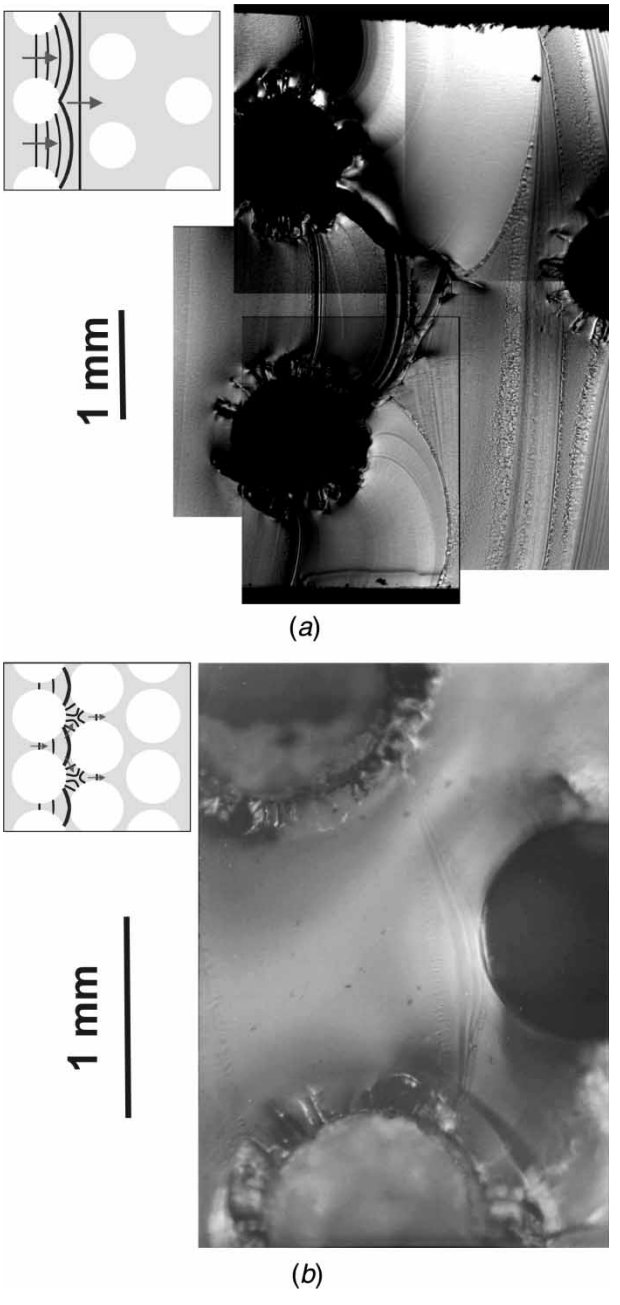

Figure 7. (*a*) Crack growth through a pore distribution when the pore volume fraction is low; (*b*) crack growth through a pore distribution when the pore volume fraction is high.

in the same way. As shown in figure 8(*a*), fracture tails and markings indicating the position of the crack front as it is growing between the pores are clearly present, which confirms that the mechanism of interaction observed here in a brittle amorphous model material is also present in a polycrystalline ceramic consistent with other observations in alumina (Passmore *et al.* 1965). A comparison with the fracture

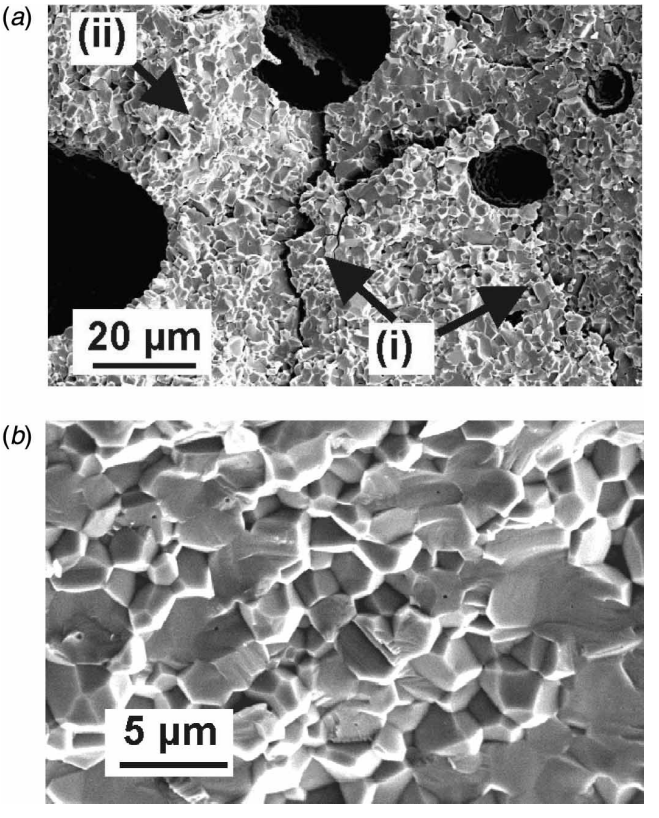

Figure 8. (*a*) Detail of a fracture surface of a sample with a relative density of 0.9 where the porosity was introduced using potato starch, showing (i) fracture tails behind pores which are formed when crack fronts growing either side of the pore meet up (see Passmore *et al*. (1965)) and (ii) a mark left by the crack front growing between the pores. (*b*) Detail of a fracture surface of a dense sample ($1-P > 0.99$).

surface of the dense material also confirms that the fracture surface of the matrix remains unchanged (figure 8).

§4. Estimating the magnitude of the crack–pore interaction

The experiments above have shown that cracks grow around pores consistent with observations made elsewhere in glasses and crystalline materials (Bethge 1962, Kerkhof and Sommer 1964, Peter 1968, Green 1983). As the difference in crack growth rate mid-way between two pores and on the pore boundary is small (see figure 6), it is neglected, so that each segment of the moving crack front increases in length by the same amount. The shape of the crack front interacting with two spherical pores is predicted to be an ellipse with its centre at (0,0) and going through the points $x = 0$, $y = R\theta$ and $x = (w/2) - R\cos\theta$, $y = R\sin\theta$, as shown in figure 9. The expression for the ellipse is

$$\frac{x^2}{g^2} + \frac{y^2}{f^2} = 1, \tag{7}$$

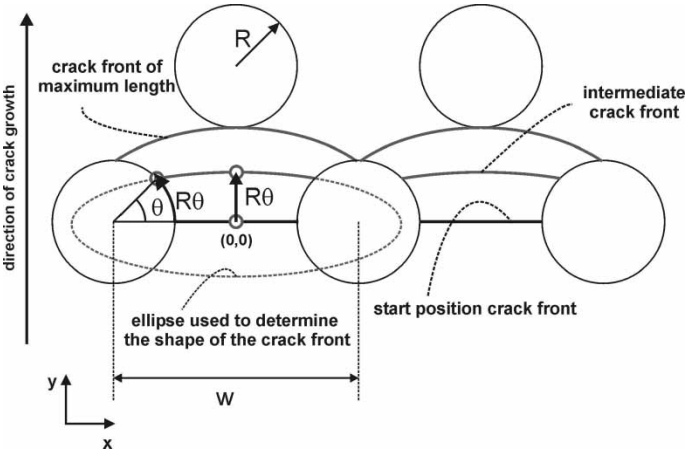

Figure 9. Three positions of the crack front. Also shown is the ellipse, which is an approximation for how the crack grows. The equation of the ellipse is obtained from the knowledge that its centre is in the middle between the two pores and from the position of two known points on its circumference. The position of these points follows from the fact that they have travelled the same total distance, one along the vertical, while the other follows the pore boundary.

where g and f are found by substitution of the coordinates of the known points

$$g = \frac{\theta[(w/2) - R\cos\theta]}{(\theta^2 - \sin^2\theta)^{1/2}}, \tag{8}$$

$$f = R\theta. \tag{9}$$

Figure 5 shows that the agreement between the experimentally observed crack front shapes and those obtained using the approximate description adopted here is reasonable.

The energy required for the crack to grow forward by a small amount is proportional to the amount of material fractured in that increment of growth and the fracture energy of the matrix. Since to a first approximation each segment of the crack front moves the same distance as the front advances, the energy required to propagate the crack front through a given amount is directly proportional to the instantaneous length of the crack front. Assuming the mechanisms contributing to the fracture energy of the matrix are not changed by the presence of pores, the maximum crack driving force needed to drive a crack past a set of pores, expressed as a fraction of that required in the dense material, is then given by

$$\frac{R_p}{R_d} = \frac{l_{max}}{w}, \tag{10}$$

where R_p is the fracture energy of the porous material, R_d is the fracture energy of the matrix, w is the width of a unit cell and l_{max} is the maximum length of the crack front.

Calculating the effect of an increase in crack front length is equivalent to considering the crack front to have a line tension as proposed by Lange (1970). However, Lange used a criterion for the maximum crack length inconsistent with observations and counted both the energy needed to create new surface during fracture, as well as an additional energy associated with the length of the crack

front. Evans (1972) has already pointed out that there is no energy directly related to the presence of a length of crack analogous to the energy of a dislocation.

In the case of a porous body, the crack must repeatedly pass between pairs of pores. The crack driving force required to do this can be no larger than the maximum value that has been estimated above. However, it might be less than this if excess elastic energy that builds up as the crack spreads around the pores, gives rise to kinetic energy of the sample, which in turn could be used to drive the crack after it has broken free and is moving towards the next pores. If all of this excess energy could be recovered then the measured fracture energy would be equal to the product of the fracture energy of the dense material and the area fraction of material in the crack plane. Unfortunately, it is not possible to determine how much of the kinetic energy may be stored in this way, although in the case of interfacial cracking, only about 25–30% of the excess elastic energy was recovered (Phillips *et al.* 1993a,b).

For a porous body, there are therefore two limits to the relative fracture energy that might be measured. The lower limit is given by the relative density, assuming that a crack grows on a random plane through the pore array, whereas the upper limit is given by the maximum length of crack front that occurs as the crack spreads through the array of pores.

The experiments have shown that the maximum length is limited by one of two conditions. Either the crack must spread around the entire pore boundary or it splits up into smaller segments when it reaches a pore ahead of the crack tip. Since the distance between pores depends on the pore distribution and the pore volume fraction, cracks will only impinge on other pores while interacting with a first set of pores if the pore volume fraction is higher than a critical value. Hence, up to that critical volume fraction of pores, the breakaway criterion is that the crack front segments, which are growing at either side of the pore, meet up again as in figure 7(*a*). For higher volume fractions of porosity, the maximum crack front length is determined by the distance with a pore ahead of the crack front as in figure 7(*b*). The situation depicted in figure 9 is for the critical pore volume fraction, where the crack front cuts into a pore ahead of the crack and joins on the pore boundary at the same length.

The lines in figure 4 show the predictions for the two limiting cases together with experimental data from the experiments here on alumina and in the literature for silicon carbide, gadolinium oxide and silicon nitride. The predictions for the case where none of the excess elastic energy can be recovered were made by numerically calculating the maximum crack length assuming the crack grows in a plane of high porosity where the pores are arranged in either a body cubic centred or closed packed cubic pore distribution. Estimates for the critical pore volume fraction and the geometries used are shown in the appendix.

Although there is considerable scatter in the data, it appears that in the region where the two bounds are most different, that is for pore volume fractions between 0.1 and 0.3, the data lie closer to the predictions of the maximum crack driving force, suggesting that little or none of the excess elastic energy can be recovered. In particular, it can be seen that, as the pore volume fraction increases, the fracture energy increases slightly before decreasing rapidly as the pore volume fraction exceeds approximately 0.2–0.3, in agreement with the rather simplified prediction for the maximum crack driving force.

The latter analysis predicts that the change in fracture energy due to spherical pores is controlled entirely by the volume fraction, there is no effect of pore size: an increase in pore size only results in a magnification of the unit geometry to be

analysed, but does not change the ratio of the maximum crack front length to the width of the unit cell. This is in accordance with the experimental observations that the fracture energy variation is similar for pores made by incorporating starch from different sources, which yields pore sizes varying between about 5 μm for rice starch up to about 45 μm for potato starch.

§ 5. Conclusions

When care is taken to eliminate effects of changes in the microstructure, the fracture energy of porous aluminium oxide remains approximately constant up to a pore volume fraction in the range 0.15–0.25. Experiments show that cracks spread around pores rather than cutting through them. As the rate of growth is constant along the crack front, the crack front bows, causing the driving force required to propagate the crack to increase as the crack grows around the pores. A quantitative analysis of the fracture energy is given which predicts that the fracture energy will remain almost constant up to a pore volume fraction of about 0.2, followed by a strong decrease, consistent with experimental results. Hence, the effect of the crack–pore interaction is not negligible for the fracture of porous bodies with low volume fraction of porosity. Both experiments and the analysis indicate that the size of the pores is not important as long as they are small compared with the overall sample.

APPENDIX

§ A1 Pore arrangements considered for calculating the relative fracture energy

In a face cubic centred pore distribution, the pore volume fraction, P, the pore radius, R, and the unit cell size, s, are related through

$$P = \frac{4(4\pi/3)R^3}{s^3}. \tag{A1}$$

As shown in figure A1, the width of a unit for analysis on a {111} plane amounts to

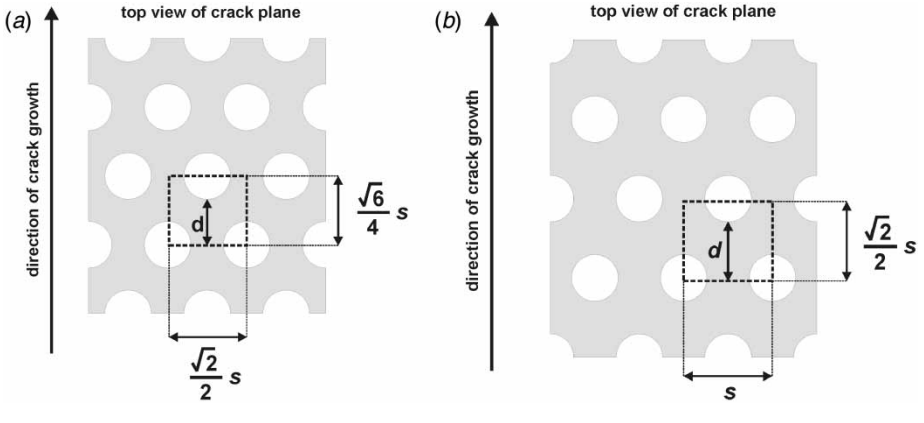

Figure A1. (*a*) Pore arrangement in a {111} plane of a face cubic centred pore distribution; (*b*) pore arrangement in a {110} plane of a body cubic centred pore distribution.

$$w = \frac{\sqrt{2}}{2}s, \tag{A2}$$

while the distance to the edge of the next pore in the centre is given by

$$d = \frac{\sqrt{6}}{4}s - R. \tag{A3}$$

The critical pore volume fraction is that pore volume fraction where growth round the pore boundary by a distance $\pi R/2$ coincides with the crack front in the centre just being able to reach the pore, or

$$\frac{\sqrt{6}s}{4} - R = \frac{\pi}{2}R, \tag{A4}$$

and therefore the critical pore volume fraction is given by

$$P_{\text{crit}} = \frac{8\sqrt{3}\pi}{\sqrt{2}(2+\pi)^3} = 0.226. \tag{A5}$$

For a body cubic centred pore distribution P, R and s are related through

$$P = \frac{2(4\pi/3)R^3}{s^3}. \tag{A6}$$

The width of a unit for analysis on a {110} plane is given by

$$w = s. \tag{A7}$$

The distance to the edge of the next pore in the centre is given by

$$d = \frac{\sqrt{2}}{2}s - R. \tag{A8}$$

And, using the same reasoning as above, the critical pore volume fraction is found as

$$P_{\text{crit}} = \frac{16\sqrt{2}\pi}{3(\pi+2)^3} = 0.174. \tag{A9}$$

References

Arato, P., 1996, *J. Mater. Sci. Lett.*, **15**, 32.

Bethge, H., 1962, *Phys. Stat. sol.*, **775**, 812.

Boccaccini, A. R., 1999, *J. porous Mater.*, **6**, 369.

Case, E. D., and Smyth, J. R., 1981, *J. Mater. Sci.*, **16**, 3215.

Coppola, J. A., and Bradt, R. C., 1973, *J. Am. Ceram. Soc.*, **56**, 392.

Daghleish, B. J., Pratt, P. L., and Sandford, J., 1976, *Science of Ceramics*, edited by P. Popper (Stoke-on-Trent: The British Ceramics Society), pp. 225–238.

Datta, S. K., Mukhopadhyay, A. K., and Chakraborty, D., 1988, *J. Mater. Sci. Lett.*, **7**, 119.

Evans, A. G., 1972, *Phil. Mag.*, **26**, 1327.

Gilman, J. J., 1959, *Fracture*, edited by B. L. Averbach, D. K. Felbeck, G. T. Hahn and D. A. Thomas (Boston: Tech. Press of MIT), pp. 193–222.

Green, D. J., 1983, *J. Am. Ceram. Soc.*, **66**, C1.

Green, D. J., Nicholson, P. S., and Embury, J. D., 1977, *J. Mater. Sci.*, **12**, 987.

Griffith, A. A., 1920, *Trans. R. Soc. Lond.* A, **221**, 163.

Johnson, K. L., Kendall, K., and Roberts, A. D., 1971, *Proc. R. Soc. Lond.* A, **324**, 301.

Kerkhof, F., and Sommer, E., 1964, *Mikroskopie in der Glas- und Emailtechnik*, vol. 4, edited by H. Freund (Frankfurt am Main: Umschau), pp. 171–192.

LAM, D. C. C., LANGE, F. F., and EVANS, A. G., 1994, *J. Am. Ceram. Soc.*, **77**, 2113.
LANGE, F. F., 1970, *Phil. Mag.*, **22**, 983; 1971, *J. Am. Ceram. Soc.*, **54**, 614.
LANKMANS, F., 1997, Master in Materials Engineering, Katholieke Universiteit Leuven, Leuven.
LAWN, B. R., and WILSHAW, T. R., 1975, *Fracture of Brittle Solids* (Cambridge: Cambridge University Press).
OSTROWSKI, T., and RÖDEL, J., 1999, *J. Am. Ceram. Soc.*, **82**, 3080.
OSTROWSKI, T., ZIEGLER, A., BORDIA, R. K., and RÖDEL, J., 1998, *J. Am. Ceram. Soc.*, **81**, 1852.
PASSMORE, E. M., SPRIGGS, R. M., and VASILAS, T., 1965, *J. Am. Ceram. Soc.*, **48**, 1.
PERRY, J. R., and DAVIDGE, R. W., 1973, *Ceramurgia*, **3**, 22.
PETER, K., 1968, *Z. angew. Phys.*, **25**, 309.
PHILLIPS, A. J., CLEGG, W. J., and CLYNE, T. W., 1993a, *Acta Mater.*, **41**, 805; 1993b, *Acta Mater.*, **41**, 819.
RICE, R. W., 1998, *Porosity of Ceramics* (New York: Marcel Dekker).
SHIGEGAKI, Y., BRITO, M. E., HIRAO, K., TORIYAMA, M., and KANZAKI, S., 1997, *J. Am. Ceram. Soc.*, **80**, 495.
SIMPSON, L. A., 1973, *J. Am. Ceram. Soc.*, **56**, 7.
SORENSEN, B. F., HORSEWELL, A., JORGENSEN, O., and KUMAR, A. N., 1998, *J. Am. Ceram. Soc.*, **81**, 661.
TATTERSALL, H. G., and TAPPIN, G., 1966, *J. Mater. Sci.*, **1**, 296.
WAGH, A. S., SINGH, J. P., and POEPPEL, R. B., 1993, *J. Mater. Sci.*, **28**, 3589.
WANG, J., VANDEPERRE, L. J., and CLEGG, W. J., 2001, *25th Annual Conference on Advanced Ceramics and Composites*, vol. 22(4), edited by M. Singh and T. Jessen (Westerville, Cocoa Beach: American Ceramic Society), pp. 233–241.
YANG, J.-F., OHJI, T., KANZAKI, S., DIAZ, A., and HAMPSHIRE, S., 2002, *J. Am. Ceram. Soc.*, **85**, 1512.
YUAN, C., 1999, Ph.D. thesis, University of Cambridge, Cambridge.